Investigación *Revista Mexicana de Física* **38**, *No. 1 (1992) 113–133*

Anomalous electron energy transport and the principle of profile consistency in TFTR transport simulations

JULIO J. MARTINELL
Instituto de Ciencias Nucleares, Universidad Nacional Autónoma de México
Apartado postal 70-543, 04510 México, D.F., México

Recibido el 28 de marzo de 1990; aceptado el 27 de septiembre de 1991

ABSTRACT. Transport simulations of several TFTR discharges using a one dimensional transport code show reasonable agreement with the experiment when the anomalous electron energy transport is modeled by an expression of the electron thermal diffusivity χ_e^{an} based on the Principle of Profile Consistency, generalized to cases with important non-Ohmic contributions to the electron energy balance, which in our case are the losses due to impurity radiation. The parameters involved in this generalization of the electron thermal diffusivity turn out to have the same values as those previously determined for Ohmic discharges in other machines such as Alcator A and FT, provided neoclassical electrical resistivity is assumed. The transport model provides a good description of electron-dominated TFTR Ohmic discharges over a range of density and plasma current. Relatively good fits to the radial electron temperature profiles and surface voltages are found for most discharges. Our results show that the total energy confinement time is in agreement with the proposed experimental scaling. They are also consistent with the scalings for the surface voltage and the electron temperature predicted by the transport model employed. The presence of sawtooth oscillations is included and it is found that, for the model we use, they have little effect on the fits to the scalings but dominate the transport in the central region of the plasma, thus affecting the profiles there.

PACS: 52.65.+z; 52.25.Fi; 52.55.Fa

1. INTRODUCTION

It is well known that the observed electron energy transport in tokamaks does not follow the predictions of the neoclassical transport theory, implying that processes other than Coulomb collisions are dominating the transport making it anomalously high. Although a great theoretical effort is being made to understand the nature of the observed transport there is still no consensus about the relevant processes and the mechanisms that produce the enhanced transport [1]. In addition to these local processes the global similarities observed in certain quantities among the different machines can be exploited in order to get some insight about the properties and general features of the anomalous transport. This idea is what has originated the formulation of the Principle of Profile Consistency [2], which relates the transport

to the observed shape of the electron temperature radial profile. In a broad sense, the basis of profile consistency is the observation that the equilibrium temperature profiles have persistently a maximum at the center of the plasma column and decrease monotonically towards the edge, for a great variety of conditions. The morphological details of the profiles (*i.e.*, trapezoidal, gaussian or other shape) depend on the machine and its operating conditions [3], but their widths seem to be controlled mainly by the safety factor q_a, regardless of the plasma size, heating method or the central temperature and density values. The use of profile consistency provides a gideline in deriving a global expression for the electron anomalous thermal diffusivity χ_e^{an} from the electron energy balance. This additional constraint, giving the variation of χ_e^{an} with r, can be used in conjunction with any local theory of anomalous transport, which would provide the magnitude of χ_e^{an} in a certain region, thus determining the termal diffusivity completely. The procedure has been applied to trapped-electron drift wave turbulence [4] and, in a heuristic way, to current-driven electrostatic modes [2], which yields the so-called Coppi-Mazzucato diffusion coefficient.

Although the significance of profile consistency has been sometimes questioned, its validity is being increasingly supported by experiments, notably in the Tokamak Fusion Test Reactor (TFTR) at the Princeton Plasma Physics Laboratory [5,6]. The observations show that electron temperature profile shapes are even more constrained than previously thought, having a weaker dependence on q_a [5], since most of the q_a dependence comes from the presence of sawtooth oscillations. These results also indicate that the current density profile $J(r)$ can be changed when decoupled from $T_e(r)$ [5], suggesting that the latter and not the former is the relevant quantity for profile consistency. This subject has been debated for some time since the two profiles are always coupled in Ohmic plasmas, through Ohm's law, but the question is not settled yet. An argument used in favor of the current density as the fundamental profile is that in currentless stellarators the T_e profile shape is dependent on the injected heating profile [7].

The expressions for χ_e^{an} that follow from profile consistency have been used in numerical simulations of discharges with only Ohmic heating obtaining a good agreement with experimental data. This was done for both the drift wave model [8] and the Coppi-Mazzucato diffusion [9,10]. the models can be modified to include non-Ohmic contributions to the electron energy balance, be them sources or sinks. Recently, this modification was incorporated to the drift wave model in simulations of TFTR discharges with injected heating [11], obtaining reasonable agreement with electron temperatures. However, the ion transport, which was also assumed to result from drift wave turbulence, gave too high ion temperatures.

The purpose of this work is to carry out a systematic numerical simulation of TFTR discharges using a profile-consistent χ_e^{an} for current-driven electrostatic modes generalized by Coppi [12] to include non-Ohmic power terms. Although we do not study plasmas with auxiliary heating, the generalized χ_e^{an} is applied to discharges with high impurity radiation losses, representing 60–95% of the Ohmic input power.

In these cases impurity radiation is a non-Ohmic sink that does not involve the additional complications that auxiliary heating processes present such as finite β_p effects or degradation of confinement. We use a one-dimensional transport code to simulate two sets of electron-dominated, Ohmic discharges in TFTR, that were performed during two operating periods (Winter of 1983-84 and Summer of 1984) characterized by high impurity content. They encompass a range of parameters wide enough to make our simulation results reliable to test the scalings implied by χ_e^{an}; typically $0.7 \leq I_P \leq 1.4$ MA at $B_T = 26$ kG and $I_P = 0.8$ MA at $B_T = 18$ kG; $1.1 \times 10^{13} \leq \bar{n}_e \leq 2.8 \times 10^{13}$ cm^{-3}; the sawtooth activity exhibited was quite diverse; and the content of impurities and radial distribution of impurity radiation showed some variation, since the two operating periods differed in the type of limiters used, being in the first set TiC-coated graphite limiters whereas the coating had been removed for the second set.

A shortcoming of the thermal transport model is that, since it is not derived directly from first principles, the magnitude of χ_e^{an} depends on a fitting constant ϵ_s (which appears also in the Ohmic case) and a normalization parameter that enters the picture when non-Ohmic energy terms are included and has to do with the power balance in a certain region of the plasma. The extent of this region and the value of ϵ_s have to be determined by comparing with experimental data. We found that ϵ_s reduces to the value previously determined for purely Ohmic discharges in Alcator A and FT [9], and Pulsator, Alcator C and other machines [10], which makes the generalized model quite appealing. The same value of ϵ_s was used for the entire series. For the normalization region we chose the entire current-carrying channel ($r \leq a_I$), since this gave the best simultaneous fit to the electron temperature profiles and loop voltage. All these determinations, as well as the whole body of the simulations, were made with the inclusion of a sawtooth oscillations model whose effect on the transport was simply to instantaneously flatten the profiles of the temperatures, particle density and current density up to a radius r_d in a periodic way, the period given by the experimental value of τ_{ST}. The disruption radius r_d of the sawtooth crash was determined from conservation of the helical magnetic flux [13], which appeared to predict the general features of the sawtooth crash and the subsequent temperature regrowth. The presence of sawtooth oscillations is important in determining the central profiles and its inclusion is essential for the fits and for reproducing certain observed features of profile consistency. For instance, the experimental result that $\langle T_e \rangle / T_{e0}$ ($\langle T_e \rangle$ is volume average) and r_d/a vary linearly with $1/q_a$ can be obtained from the simulations only if sawteeth are present.

Different choices of the electrical resistivity $\eta_{\|}$ were considered (classical, neoclassical and a mixture of them), and comparing the best fit to several discharges with each choice, we could determine the most adequate of them. The effect of varying the form of $\eta_{\|}$ could be distinguished from that due to possible different normalizations of χ_e^{an} in obtaining the best fit. We found that a neoclassical resistivity yielded a much better fit to the electron temperature profile and voltage than a purely classical resistivity. This is in agreement with the results of Zarnstorff *et*

al. [14], who found that experimental measurements of Ohmic TFTR plasmas were consistent with predictions of the loop voltage based on neoclassical resistivity and inconsistent with classical resistivity. The ion transport was not analyzed in detail but T_{i0} seemed to be reasonably well reproduced by the Chang-Hinton neoclassical ion thermal conductivity [15], and therefore we did not consider anomalous ion transport.

An important result of our work is that the values of the total energy confinement time τ_E^{OH} and the electron energy confinement time τ_{Ee} are compatible with the observed experimental scaling given in terms of fundamental plasma parameters. They are also in rough agreement with the theoretical scaling predicted by the model, which is not expressable in a simple form and thus it cannot be directly related to the experimental scaling. Our results are also consistent with the theoretical predictions for the scalings of the surface voltage V_s and the central electron temperature in a much better way than they are for τ_{Ee}. Since the τ_{Ee} predicted scaling is obtained from that for V_s, this implies that τ_{Ee} is harder to predict theoretically because the "errors" in the surface voltage scaling are amplified when they enter τ_{Ee}. This result together with the fact that there are many possible forms of χ_e^{an} that give the same τ_{Ee} scaling, imply that it is not possible to use the energy confinement time as a quantity to predict the form of χ_e^{an}. This conclusion seems to be independent of whether sawteeth are present or not since they do not modify the scalings in a significant way within the model we considered.

We next present the method of analysis and the results in some detail. Section 2 describes the complete transport model and the choice of χ_e^{an} without getting into the details of its derivation and fundamentation; this is discussed in Ref. [12]. In Section 3 the results of the simulations are presented and the quality of the overall fit is discussed. Section 4 is devoted to analyze the implications of the results and the meaning of the energy confinement time scaling as a predictive tool. The conclusions are summarized in the last section.

2. THE SIMULATION

2.1. The numerical model

A complete predictive transport simulation should predict the time evolution of the plasma parameters such as the surface loop voltage V_s, the toroidal current density j_z, the particle temperatures T_e and T_i, and the densities n_e and n_i of the main plasma species, given the initial and boundary conditions, by using only the self-contained models. In practice the simulation is incomplete and the effects of a number of processes must enter through independent parameters determined from experimental observation. For the cases considered here, time evolution equations for n_i ($\sim n_e$), T_e, T_i, and the poloidal magnetic field B_P were solved in cylindrical geometry. The major effects that were calculated explicitly were the energy sources

and sinks, with the exception of the impurity radiation loss, the neoclassical transport of electrons and a mixture of H and D ions and of their thermal energy, the anomalous electron thermal diffusion, an anomalous outward and inward particle flux, central sawtooth crashes at regular intervals, and a hydrogenic neutrals profile that was normalized so that the ionization rate exactly compensated for the ion outflow at the plasma edge.

The independent initial parameters were the total number of electrons specified by the profile $n_e^0(r)$, the geometrical major radius R, the limiter minor radius a, the vacuum toroidal magnetic field B_T at R, and the total plasma current I_P. The sawtooth period τ_{ST} was fixed at the average experimental value for a complete reconnection cycle. Additional parameters that were treated as independent, but that in reality varied systematically with $\bar{n}_e$ (line-averaged electron density) or I_P described the plasma composition. The effective charge Z_{eff} was taken from the visible bremsstrahlung emission, and, along with the ratios $n_D/(n_H + n_D)$ and $(n_H + n_D)/n_e$ determined from spectroscopic data, was taken to be fixed in time and constant across the plasma cross section. The total volume-integrated impurity radiation loss $P_R \equiv \int_{r=0}^{a} S_R(r)\, d^3r$ and the Abel inverted emissivity profile $S_R(r)$ were taken from bolometer measurements [16]. The temperatures $T_e(r)$ and $T_i(r)$ and the inverse rotational transform $q(r)$ were also specified initially, but rapidly evolved toward steady state values. The edge temperatures T_{ea} and T_{ia} were fixed in time. The initial edge density was chosen to be $0.2n_{e0}$, but the boundary condition was $\partial n/\partial r(a) \approx 0$.

The numerical fit proceeded as follows. Values of Z_{eff} and a constant of proportionality multiplying $S_R(r)$ were varied to yield the best match to experimental values of $T_e(r)$, T_{i0}, V_s, and $\tau_E^{OH} \equiv (3/2)\int_{r=0}^{a}(n_eT_e + n_iT_i)\, d^3r / \int_{r=0}^{a} E_{\|}J_{\|}d^3r$, all averaged over a sawtooth period. The initial particle density and numerical factor c_p multiplying the anomalous inward particle flux [cf. Eq. (11)] were chosen to reproduce the measured $\bar{n}_e$ and either a value of $n_{e0} \equiv n_e\ (r = 0)$ that was not too different from a parabolic $n_e(r)$ profile if no additional data was available, or was compatible with the instantaneous Thompson scattering (TVTS) profile measured at random phase on a sawtooth oscillation. The edge temperatures T_{ea} and T_{ia} were varied to provide the best overall fit to the profiles, the Ohmic heating and the surface voltage. Matching the observed electron temperature profile constituted a major part of the fit; the best match was not always determined by the value of T_{e0}. The remainder of this section describes in detail the assumptions made about the processes directly affecting the profiles.

2.2. Sawtooth oscillations

Sawtooth oscillations determined the central width of the electron temperature profile and the toroidal current density for $I_P \geq 1$ MA. The sawtooth model triggered an instantaneous crash at intervals $\Delta t = \tau_{ST}$, the observed sawtooth period, which ranged from some 20 ms for a low current sawtooth up to 60 ms for the full recon-

nection cycle of a compound sawtooth. The period could not be predicted a priori because of a lack of knowledge concerning the physical mechanism of the sawtooth oscillations (see, *e.g.*, Ref [17]). The disruption radius r_d and the redistribution of j_z and B_P were determined from the self-consistent computed $j_z(r)$ by assuming helical flux conservation as in Kadomtsev's model [13]; the helical flux was corrected for noncylindrical effects by taking $B_P = B_P^{\mathrm{cyl}}/(1+\alpha r/a)$, where α was determined from measurements of the magnetic $q_\psi(a)$. The resulting j_z profiles are flat to slightly hollow inside r_d at the higher currents (1.4 MA). They become significantly hollow at yet higher current. The profiles T_e, T_i and n_e (n_i) were flattened inside r_d while conserving particles inside that radius and depositing the helical magnetic energy released by the reconnection as kinetic energy in the electrons and ions equally distributed. Hollow and flattened T_e and T_i profiles cannot be distinguished on the basis of experimental data at these currents [18], and the density does not change greatly during a crash. By assumption, the impurity ion concentrations, which appear only through Z_{eff} in the simulation, are not changed by a crash.

The reconnection always extended from the magnetic axis past the largest $q = 1$ surface. Although both experiment [17,18] and numerical simulations such as the present one [19] indicate that partial reconnections are likely to occur at higher currents and densities, perhaps due to the development of nonmonotonic q profiles and multiple $m = 1$ magnetic islands, the energy balance in this discharges with moderate sawteeth seems to be accurately simulated by ignoring the intermediate reconnections. In fact, over the range of current and density, this model gives reasonable fits to the inversion radius r_i as measured by soft X-ray emission [20] and by ECE radiometer [18], and also to r_d as estimated from the central width of the time-averaged ECE radiometer $T_e(r)$ profiles. Helical flux conservation has been shown to give the correct qualitative variation of r_d with q_a when used with other forms of χ_e^{an} (*e.g.*, Ref. [9]), but the absolute size depends upon χ_e^{an} and other factors. At higher currents or with larger sawteeth, however, partial reconnection may become an important factor in the Ohmic heating.

2.3. Electrical resistivity

In steady state the electron temperature and the parallel current density are coupled through an Ohm's law. In all the cases reported here the plasma electrical resistivity $\eta_{\|}$ was assumed to be neoclassical outside $r = r_s$, the instantaneous location of the $q = 1$ surface determined from the transport solution for $j_z(r)$. An entirely classical resistivity yielded unsatisfactorily low temperatures and low voltages for reasonable values of Z_{eff} and P_R. When the resistivity was assumed to be neoclassical outside r_s and either classical or neoclassical inside r_s reasonably good fits were obtained, with the completely neoclassical choice coming closer to the experimental observations for the higher current cases that had larger sawteeth. The same conclusion was reached in Ref. [14].

2.4. *Electron thermal diffusion*

The local expression for the electron thermal diffusivity χ_e^{an} is derived from the principle of profile consistency and therefore is directly dependent upon the balance of all the energy sources and sinks. Its actual value depends on a normalization constant that can only be determined by comparison with experiment and thus reflects the total content of the simulation code. We will briefly mention how χ_e^{an} is derived in cylindrical geometry when non-Ohmic sources and sinks are present, represented by a term $S^e(r)$. The derivation for general flux surface geometry as well as a detailed discussion of it are given in Ref. [12]. The steady state electron energy balance is written as

$$\frac{1}{r}\frac{d}{dr}\left(r\kappa\frac{dT_e}{dr}\right) = E_{\|}J_{\|} + S^e(r). \tag{1}$$

Invoking profile consistency a centrally peaked form of the parallel current density is taken as $J_{\|}(r) = J_0 \exp(-\alpha_J \ell(r^2/a_I^2))$, where $\ell(\zeta) \simeq \zeta$, outside the sawtooth region. Writing $J_{\|}$ in terms of T_e through the neoclassical Ohm's law $E_{\|} = \eta_{\|}J_{\|} = \hat{\eta}T_e^{-3/2}f_T^{-1}J_{\|}$, with $E_{\|}(r) \simeq$ const. in a strict steady state without sawteeth, we can evaluate the gradient dT_e/dr in Eq. (1) and find for $\chi_e^{an} \equiv \kappa/n$ the expression [12]

$$\chi_e^{an}\,(\mathrm{cm}^2/\mathrm{s}) = 1.23 \times 10^{13}\epsilon_s \frac{a_I I_P}{r^2}\frac{W_N(r)}{T_e(r)n_e(r)^{4/5}}\left(\frac{\lambda_{ei}Z_*}{A_i}\right)^{2/5} F(\beta_p^e), \tag{2}$$

$$W_N(r) = \frac{\int_0^r (E_{\|}J_{\|} + S^e(r_0))r_0 dr_0}{\int_0^{a_I} E_{\|}J_{\|}r_0 dr_0 + \frac{I_P}{I_{\|}(r_*)}\int_0^{r_*} S^e(r_0)r_0 dr_0}. \tag{3}$$

Here $F(\beta_p^e)$ represents a function accounting for the degradation due to finite β_p which is not of importance in our case and then we will set $F(\beta_p^e) = 1$; $Z_* \equiv A_i \sum_j Z_j^2 n_j/(n_e A_j) \simeq Z_i$ (main species); r_* represents the extent of the normalization region; ϵ_s is a constant of order one to be determined; A_i the atomic weight of the main species ions in amu; λ_{ei} the Coulomb logarithm; I_P in kA the total plasma current carried inside the current channel $r \leq a_I$; n_i the main ion species density in cm^{-3}; and T_e is in keV.

The magnitude and scalings of χ_e^{an} with the plasma parameters as given in Eq. (2) were obtained by assuming the transport results from current-driven electrostatic modes, which are heuristicaly introduced through a dimensionless number C_s representing the ratio of anomalous to classical diffusion as [12]

$$C_s = \frac{\nu_{ee}}{v_{\mathrm{the}}^2} d_e^2 \nu_{\mathrm{eff}} \quad \text{with} \quad \nu_{\mathrm{eff}} = \omega_{pi}\frac{v_s}{v_{th_e}}, \tag{4}$$

where d_e is the electron inertial skin depth ν_{ee} the electron-electron collision frequency, ω_{pi} the ion plasma frequency, v_{the} the electron thermal speed and ν_{eff} represents and effective rate of momentum transfer which is characteristic of electrostatic current driven modes [21]. The normalization of W_N to the radius r_* has several theoretical possibilities. It directly determines the expected value of the steady state loop voltage, given the Ohmic scaling through $\bar{\bar{V}}$:

$$V_{\|} = \epsilon_s \bar{\bar{V}} \frac{R}{4a_I} - \frac{1}{I_{\|}(r_*)} \int_0^{r_*} S^e(r_0) r_0 dr_0, \tag{5}$$

$$e\bar{\bar{V}} = \frac{1}{\int_0^1 d(\frac{r}{a})^2 (T_e C_s^{2/5})^{-1}}.$$

The increase in $V_{\|}$ resulting from an energy sink $[S^e(r) = -S_R(r)]$ plays an important role in matching the surface voltages observed in TFTR discharges with large radiation losses. Simultaneous fits to T_e and V_s showed that $r_* = a_I$ gave better results than taking into account only the central energy balance, through choices such as $r_* = r_s$ or $r_* = 0$ [for the latter the denominator in Eq. (3) is taken as $\int_0^{a_I} E_{\|} J_{\|} r dr + (a_I^2/2) S^e(0)$].

Now, in cases where Ohmic heating dominated the electron energy balance and sawtooth oscillations, if present, were small (Alcator A and FT), the constant factor ϵ_s that scales the loop voltage has been found to have a value 0.25–0.32 for D plasmas, increasing with $q(a)$ [9]. Varying the magnitude by $\pm 25\%$ produced a $\pm 10\%$ variation in T_{e0}. Values close to 0.25 fit Ohmic discharges in Alcator C, Pulsator and FT [10], when embedded in other transport codes. The diffusion dominated interval of the minor radius in ASDEX Ohmic discharges, $r_s \leq r \leq 36$ cm ($a = 40$ cm), has been fit by $\epsilon_s \simeq 0.5 - 0.65$ when combined with other expressions for χ_e^{an} in the other intervals [22]. For the TFTR cases simulated here we used the value $\epsilon_s = 0.25$ but a variation of almost $\pm 40\%$ was found to produce changes of only $\pm 10\%$ in T_{e0}.

In cases dominated by Ohmic heating the model for χ_e^{an} implies the equilibrium scalings [12]

$$T_e^{OH} \sim n_e^{-2/15} B_P^{2/3} Z_{\text{eff}}^{2/3} \left(\frac{A_i}{Z_i}\right)^{4/15} \left(\frac{n_e}{n_i}\right)^{2/15} \left(\frac{a}{a_I \epsilon_s}\right)^{2/3}, \tag{6}$$

$$V_{\|}^{OH} \sim \epsilon_s \left(\frac{R}{4a_I}\right) \left(\frac{A_i}{Z_i}\right)^{-2/5} n_i^{1/5}, \tag{7}$$

$$\tau_{Ee}^{OH} \sim n_e^{2/3} a^2 B_P^{-1/3} Z_{\text{eff}}^{2/3} \left(\frac{A_i}{Z_i}\right)^{2/3} \left(\frac{n_e}{n_i}\right)^{1/3} \epsilon_s^{-5/3} \left(\frac{a_I}{a}\right)^{1/3}, \tag{8}$$

where $B_p = B_p(a)$. In the case that the non-Ohmic terms dominate, the corresponding scalings equivalent to Eqs. (6)–(8) can also be derived [12], but in the

intermediate situation where Ohmic and non-Ohmic terms are of the same order no simple scalings exist. In this case however, implicit scalings for T_{e0} and τ_{Ee} can be obtained in terms of the total $V_{\|} = V_{\|}^{OH} + V_{\|}^{NOH}$ as given by Eq. (5), which depends on the relative size of Ohmic $V_{\|}^{OH}$ and non-Ohmic $V_{\|}^{NOH}$ terms. We find

$$T_e \sim T_e^{OH} \left(\frac{V_{\|}^{OH}}{V_{\|}^{OH} + V_{\|}^{NOH}} \right)^{2/3}, \tag{9}$$

$$\tau_{Ee} \sim \tau_{Ee}^{OH} \left(\frac{V_{\|}^{OH}}{V_{\|}^{OH} + V_{\|}^{NOH}} \right)^{2/3} \frac{1}{W_N(r = \tilde{r})}. \tag{10}$$

where T_e^{OH} and τ_{Ee}^{OH} are the scalings of Eqs. (6) and (8) and $\tilde{r}$ is the particular radius at which τ_{Ee} is to be evaluated [we use $\tilde{r} \simeq (2/3)a$].

2.5. Particle transport

The electrons and the main species ions were assumed to experience a neoclassical Ware pinch, and in addition an anomalous outward and inward flow that is related to the anomalous electron thermal diffusion. This flux can be written as

$$\Gamma_{\text{an}} = -D_p \left(\frac{\partial n_e}{\partial r} - 2 n_e \alpha_p \frac{r}{a^2} \right), \tag{11}$$

where $\alpha_p(r) = c_p(1 + 4.1(\nu_e^{**})^{1/2})$, $\nu_e^{**} = \nu_{ei}(Rq/v_{\text{the}})(1 + Z_{\text{eff}}/2)$, ν_{ei} is the electron ion collision frequency, and c_p is a numerical constant of order one that controls the magnitude of the inward pinch. This expression generalizes the one presented in Ref. [23] to less collisional regimes, in a heuristic manner. The particle diffusion coefficient is chosen to be $D_p = 0.2\chi_e^{\text{an}}$, from comparison with many different experiments. The results are not sensitive to the exact shape of the density profile.

In addition to the neoclassical and anomalous electron thermal diffusion, both electrons and ions underwent thermal transport due to convection, assumed to have the form $(5/2)n_j T_j v_j$.

3. THE RESULTS

Current and density scans of full-size ($R \simeq 255$ cm, $a \simeq 80$ cm) Ohmic plasmas were selected from two operating periods, the summer of 1984 when graphite limiters were used and therefore produced low Z impurities [24] (series 1), and the winter of 1983-84 when TiC-coated graphite limiters introduced a comparatively large content of high Z impurities [25] (series 2). Representative cases were then simulated

with the predictive transport model. The normalization of W_N introduced into the anomalous electron thermal diffusivity by the presence of non-Ohmic source terms Eq. (3), was determined from series 1 and applied to series 2 to test its adequacy. As mentioned above the best normalization was for $r_* = a_I$. In all cases, the best fits assumed that $\eta_{||}$ was uniformly neoclassical over the plasma cross section.

3.1. Series 1

For this series the sawtooth-averaged experimental values of $T_e(r)$, V_s and τ_E^{OH} were fit within $\pm 10\%$ for values of Z_{eff} and P_R that were in the $\pm 10\%$ range of the measured values, for about 60% of the discharges modeled. For the rest, at least one of these two parameters had larger departures. The results for selected discharges are summarized in Table I. All quantities above the horizontal line were given as input to the code. In all cases we used for the current carrying radius $a_I = a$. The resulting $T_e(r)$ steady state profiles for representative discharges of this series are shown in Fig. 1, at four times during the sawtooth cycle, namely, $t = (0.0, 0.05, 0.5,$ and $0.95) \times \tau_{ST}$ after a sawtooth crash. For comparison, the experimental profiles averaged over sawteeth are shown by the circles. For currents of 1.0 MA or larger the profiles are relatively well fit but for high values of the limiter q the simulation profiles are somewhat wider than those obtained experimentally. The same disagreement for large q_a has been reported in Refs. [5,6], when experimental temperature profiles are fit by gaussian-like profiles. This means that the shape assumed for $T_e(r)$ in the derivation of χ_e^{an} is not so adequate at large q_a.

The total energy confinement time based upon the Ohmic power, τ_E^{OH} given in Table I is computed with the same expression the TFTR team used [25] which in steady state is $\tau_E^{OH} = (3/2) \int_{r=0}^{a} (n_e T_e + n_i T_i) d^3r / \int_{r=0}^{a} E_{||} J_{||} d^3r$. It essentially corresponds to the ratio of β to the Ohmic power, and both of these quantities are matched within $\pm 10\%$, which makes τ_E^{OH} to be also in good agreement with the experiment. The fact that β has the right value means that the temperature profiles are acceptable. This is true even for the high q cases where $T_e(r)$ seemed to be too wide.

The central ion temperatures deduced from the measured neutron flux were generally reproduced within $\pm 10\%$ assuming the ion thermal conductivity to be equal to the Chang-Hinton [15] (neoclassical) value χ_i^{CH}. We point out though, that the experimental T_{i0} values were usually selected from discharges that assumed low values of the neoclassical multiplier (≤ 3) in the data analysis, and this probably weighted χ_i towards $1 \times \chi_i^{CH}$. In any case, given that we did not put any special attention to fitting T_{i0}, the $\pm 10\%$ agreement is quite good.

3.2. Series 2

In this series there are several cases where the impurity density becomes comparable to that of the hydrogenic ions [very low $(n_H + n_D)/n_e$], especially at low currents,

Discharge	9970		9818		9961		9816		9942		9922		9925	
	Exper.	Simul.	Exper.	Simul.	Exper.	Simul.	Exper.	Simul.	Exper.	Simul.	Exper.	Simul.	Exper.	Simul.
I_P (MA)	0.7	0.7	1.0	1.0	1.0	1.0	1.0	1.0	1.4	1.4	1.4	1.4	1.4	1.4
R (cm)	255	255	255	255	255	255	255	255	255	255	255	255	255	255
a (cm)	82.4	82.4	82.4	82.4	82.4	82.4	82.4	82.4	82.3	82.3	82.4	82.4	82.4	82.4
B_T (kG)	27.9	27.9	27.9	27.9	27.9	27.9	27.9	27.9	27.9	27.9	27.9	27.9	27.9	27.9
Z_{eff}	3.85	3.9	5.7	6.8	4.8	4.1	3.5	3.9	6.85	6.2	3.75	3.4	3.4	3.4
P_R (MW)	0.34	0.3	0.69	0.66	0.60	0.61	–	0.53	0.71	0.93	0.86	0.85	0.89	0.95
τ_{ST} (ms)	23	23	28	25	25	25	35	35	26	26	32	32	60	60
T_{ea} (eV)		120		400		220		220		200		160		250
$\frac{(n_H+n_D)}{n_e}$	0.55	0.55	0.35	0.35	0.41	0.41	0.54	0.54	0.26	0.26	0.62	0.62	0.67	0.67
$\frac{n_D}{(n_H+n_D)}$	0.79	0.79	0.70	0.70	0.78	0.78	0.80	0.80	0.77	0.77	0.78	0.78	0.78	0.78
$\bar{n}_e$ (10^{13} cm^{-3})	1.26	1.27	1.14	1.17/1.16	1.51	1.54/1.52	2.11	2.12/2.10	1.39	1.42/1.41	2.41	2.44/2.41	2.72	2.75/2.68
n_{e0} (10^{13} cm^{-3})	1.83	1.83/1.78	1.65	1.75/1.65	2.20	2.32/2.19	3.06	3.22/3.02	2.0	1.86/1.75	3.60	3.23/3.04	3.9	4.06/3.61
T_{e0} (keV)	2.26	2.34/2.26	3.38	3.43/3.22	2.46	2.60/2.40	2.53	2.51/2.31	3.45	3.88/3.40	2.40	2.61/2.28	2.45	2.58/2.15
		⟨2.32⟩		⟨3.36⟩		⟨2.54⟩		⟨2.45⟩		⟨3.64⟩		⟨2.45⟩		⟨2.40⟩
T_{i0} (keV)	1.77	1.70/1.69	2.37	2.62/2.46	2.16	2.20/2.04	1.85	2.12/2.02	2.89	3.29/2.80	2.16	2.26/2.08	1.72	2.33/2.03
V_s (V)	0.77	0.75	0.9	0.88	0.89	0.87	0.83	0.83	1.05	1.0	1.01	1.0	1.01	1 0/0.99
P_{OH} (MW)	0.54	⟨0.54⟩	0.9	⟨0.88⟩	0.89	⟨0.87⟩	0.83	⟨0.83⟩	1.47	⟨1.37⟩	1.41	⟨1.39⟩	1.42	⟨1.38⟩
β (10^{-3})	0.75	⟨0.79⟩	1.02	⟨1.11⟩	1.12	⟨1.11⟩	1.58	⟨1.62⟩	1.40	⟨1.52⟩	2.16	⟨2.22⟩	2.35	⟨2.52⟩
τ_E^{OH} (ms)	220	⟨234⟩	180	⟨199⟩	199	⟨202⟩	301	⟨309⟩	151	⟨176⟩	243	⟨253⟩	262	⟨290⟩
R_i (cm)	17	8.5	22	14.2	22	15.6	22	15.6	27.5	30.2	27.5	28.3	25.0	26.6
r_d (cm)		12.4		20.6		22.7		22.7		41.2		39.1		39.1

TABLE I. Simulation results for TFTR discharges in the operating period of the summer of 1984, with graphite limiters. ⟨ ⟩ means average over sawtooth period.

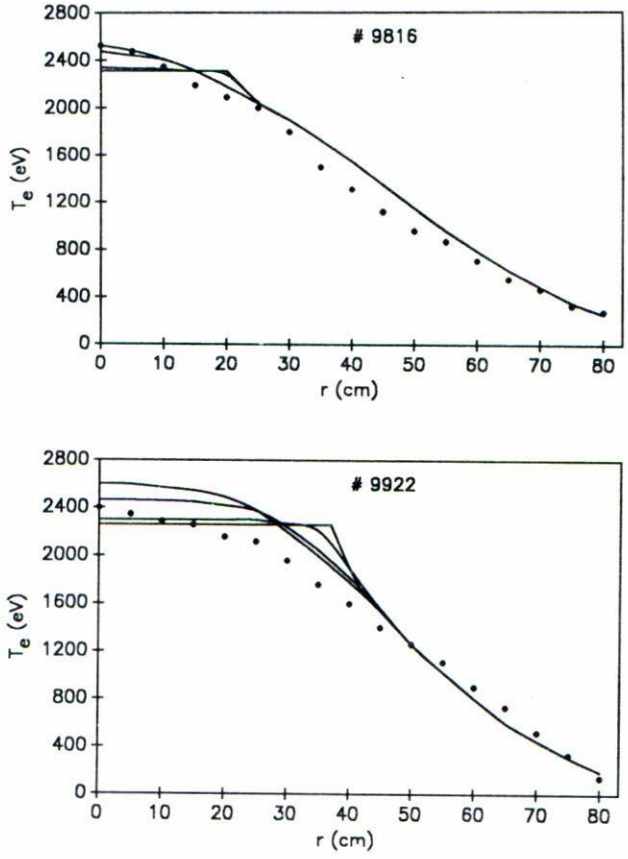

FIGURE 1. Comparison of simulation and experimental results for sample discharges of the summer period. Solid lines represent simulation electron temperature profiles at four different times in a sawtooth period. Circles give measured profiles representing sawtooth-averaged values.

and these cases constitute the most severe test of the anomalous transport model. At very low values of $(n_H + n_D)/n_e$ the main problem with the transport model is that it assumes there is only one species of main ions ($Z = 1$) and then when another species becomes comparable to them this approximation breaks down. Our results, however, show that the approximations concerning high concentrations of heavy impurities are not so bad since acceptable fits can be found.

The results for selected discharges of series 2 are given in Table II. We obtain that the values of T_{e0} and V_s are always within ± 13–15% of the experimental ones, which is accomplished with Z_{eff} and P_R within a $\pm 15\%$ range for all but one of the discharges. Although for most cases we used $a_I = a$, the possibility of having $a_I < a$ was considered when the measured $T_e(r)$ was narrow enough, in order to improve the fit. Only in one of the discharges this was actually needed. Sample $T_e(r)$ profiles for this series are shown in Fig. 2. The edge temperature T_{ea} was

Discharge	8819		8803		8827		9040		9063		9068	
	Exper.	Simul.	Exper.	Simul.	Exper.	Simul.	Exper.	Simul.	Exper.	Simul.	Exper.	Simul.
I_P (MA)	0.99	0.99	0.99	0.99	0.99	0.99	1.2	1.2	1.29	1.29	1.39	1.39
R (cm)	266	266	266	266	266	266	256	256	265	265	263	263
a (cm)	76.3	76.3	76.3	76.3	76.3	76.3	81.7	81.7	77.2	77.2	78.0	78.0
B_T (kG)	26.3	26.3	26.3	26.3	26.3	26.3	26.9	26.9	26.5	26.5	26.6	26.6
Z_{eff}	5.51	5.0	3.88	3.5	3.16	2.84	3.47	3.12	3.58	2.74	4.13	3.6
P_R (MW)	0.72	0.65	0.59	0.60	0.51	0.48	1.09	1.17	1.08	0.94	1.27	1.29
τ_{ST} (ms)	22	22	36	36	22	22	31	31	32	32	36	36
T_{ea} (eV)		200		160		200		150		150		200
$\frac{(n_H+n_D)}{n_e}$	0.54	0.54	0.66	0.66	0.75	0.75	0.68	0.68	0.67	0.67	0.62	0.62
$\frac{n_D}{(n_H+n_D)}$	0.78	0.78	0.78	0.78	0.78	0.78	0.85	0.85	0.85	0.85	0.85	0.85
$\bar{n}_e$ (10^{13} cm^{-3})	1.69	1.74/1.72	2.28	2.34/2.30	2.86	2.89/2.86	2.33	2.36/2.33	2.45	2.43/2.39	2.50	2.51/2.46
n_{e0} (10^{13} cm^{-3})	2.3	2.26/2.15	3.30	3.30/3.12	4.1	3.84/3.65	3.40	3.33/3.13	3.60	3.14/2.94	3.60	3.28/3.02
T_{e0} (keV)	2.50	2.77/2.46	2.07	2.26/2.0	1.74	2.0/1.78	1.92	2.15/1.87	1.91	2.05/1.75	1.98	2.24/1.86
		⟨2.62⟩		⟨2.12⟩		⟨1.89⟩		⟨2.02⟩		⟨1.90⟩		⟨2.06⟩
T_{i0} (keV)	1.96	2.19/2.02	1.76	1.95/1.80	1.55	1.75/1.62	1.64	1.89/1.73	1.66	1.80/1.63	1.71	1.97/1.73
V_s (V)	1.0	1.05	0.93	1.01/1.0	0.97	1.01	1.07	1.08	1.05	1.15/1.14	1.16	1.32/1.30
P_{OH} (MW)	1.0	⟨1.03⟩	0.92	⟨0.99⟩	0.96	⟨1.0⟩	1.28	⟨1.29⟩	1.35	⟨1.45⟩	1.61	⟨1.79⟩
β (10^{-3})	1.62	⟨1.71⟩	2.03	⟨2.04⟩	2.24	⟨2.30⟩	1.68	⟨1.88⟩	2.23	⟨2.15⟩	2.17	⟨2.35⟩
τ_E^{OH} (ms)	204	⟨211⟩	278	⟨260⟩	296	⟨291⟩	192	⟨213⟩	214	⟨193⟩	188	⟨175⟩
r_i (cm)		23.2		21.5		23.3		24.3		30.5		31.7
r_d (cm)		32.4		30.5		32.4		34.7		42.5		44.9

TABLE II. Simulation results for TFTR discharges in the operating period of the winter of 1983-84, with TiC-coated graphite limiters.

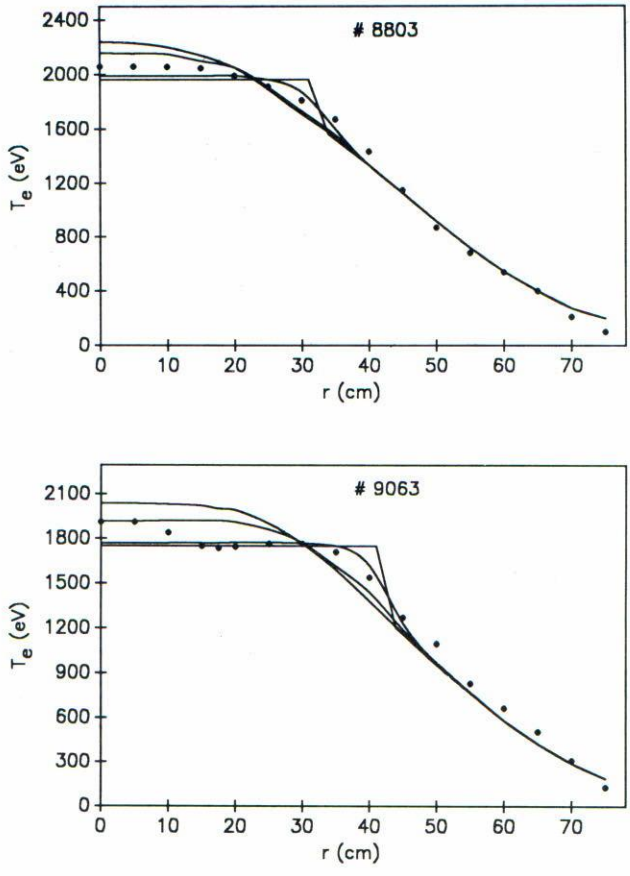

FIGURE 2. Same as Fig. 1, for sample discharges of the winter period.

generally quite high compared to the experimental value when the overall profile was fit, but this is not an experimentally accurate quantity and the discrepancy is not very significant. As in the cases of series 1, the values of T_{i0} are usually within the $\pm 10\%$ range of the experimental data when we take $\chi_i = \chi_i^{\mathrm{CH}}$.

We should mention that, although the value of V_s falls normally within the $\pm 10\%$ range, it is generally overestimated by the simulation, especially for low currents. In this series, however, we did not vary the normalization of W_N as we did with series 1, when finding the best value for r_*. Thus this result might be indicative of some deficiency of the normalization for this series, but it is still remarkable that the same normalization can be used for two series of discharges with comparatively different properties.

For both series, in obtaining the best fits it was found that the code results were most sensitive to variations of the parameters Z_{eff} and P_R. The sensitivity to Z_{eff} and the relatively high impurity content imply that the results may be affected by

spatial variations in Z_{eff} and $(n_H + n_D)/n_e$ but there is no experimental data for comparison.

4. ANALYSIS AND DISCUSSION

The analysis of the experimental TFTR results has showed that the total energy confinement time scales with the fundamental plasma parameters as [24,25]

$$\tau_E \sim \bar{n}_e q_a a R^2. \tag{12}$$

In the results presented above the value of τ_E^{OH} is usually within a $\pm 10\%$ range of the experimental value and thus it would not be surprising for it to follow the experimental scaling. In Fig. 3(a) we plot τ_E^{OH} from the simulations against the scaling (12) to test this conjecture, and find that it is obeyed to a reasonably good degree (0.85 correlation). On the other hand, for electron dominated discharges one would expect τ_E^{OH} to follow one of the theoretical scalings given by Eq. (8) in the purely Ohmic case or Eq. (10) in the general case, which are quite different from Eq. (12).

However, even for electron dominated experiments we have to distinguish between τ_E^{OH} and the electron energy confinement time τ_{Ee}, which is the one that can be directly predicted from χ_e^{an}. We define τ_{Ee} as

$$\tau_{Ee} = \frac{(3/2)\int_{r=0}^{2a/3} n_e T_e d^3r}{\int_{r=0}^{2a/3}(E_{\|}J_{\|} - S_R - P_{ei} - P_{\text{conv}})d^3r}, \tag{13}$$

where we took the volume up to $r = 2a/3$ to minimize edge effects resulting from the boundary conditions chosen. We included all the relevant energy sources and sinks in the definition to make sure they are not the cause of any difference in scaling. Now we can check if τ_{Ee} also follows the scaling (12), which we do in Fig. 3(b). This time the correlation is not so good (only 0.66) indicating that there is a difference between τ_{Ee} and τ_E^{OH}, probably due to the exclusion of the non-Ohmic terms in the definition of τ_E^{OH}, which is a simplified confinement time. Then in order to compare with the scalings predicted by χ_e^{an} we should not use τ_E^{OH} but τ_{Ee}.

In order to check the consistency of our results we compared the predicted scalings of Eqs. (5), (9) and (10) with the corresponding values from the simulations. When this is done for the loop voltage and the electron temperature the agreement is remarkably good, with correlations of 0.94 and 0.96 respectively, which indicates that the results are self-consistent. However, for τ_{Ee} the correlation is not very good (only 0.73). We show this plot (τ_{Ee} from the simulation *vs.* theoretical scaling of Eq. (10)) in Fig. 4(a). Thus, the good correlation found for V_s and T_e is somewhere weakened when they are combined to produce the scaling (10) for τ_{Ee}. It is then

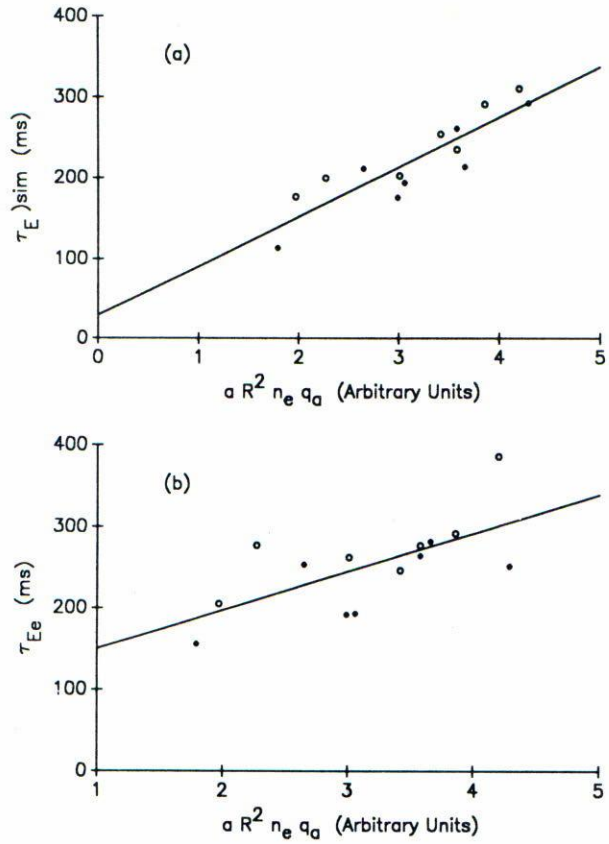

FIGURE 3. Relation between simulation confinement time and the resulting experimental scaling $aR^2n_eq_a$. Open and filled circles represent discharges from the summer and winter periods respectively (a) For the total energy confinement time τ_E the least squares fit correlation is 0.85; (b) and for the electron energy confinement time τ_{Ee} it is 0.66.

important to find out why this happens. From the definition (13) we notice that $\tau_{Ee} \sim n_eT_ea^2R/(P_{OH} - P_R)$ which gives the result (10) when the scalings for T_e and $V_s(= P_{OH}/I_P)$ are used. If we use this relationship substituting only the temperature scaling and take the value of $P_{OH} - P_R$ directly from the numerical results we can get a partial scaling that we can test. When this is compared with τ_{Ee} from the simulations the agreement is remarkably good as it is shown in Fig. 4(b), having a correlation of 0.99. This means that variations in the T_e or n_e profiles are not the cause of the discrepancy, but it is when the scaling for V_s is introduced that the correlation between τ_{Ee} and the predicted scaling is spoiled. This is apparently due to the fact that V_s enters the scaling of τ_{Ee} as $V_s^{-5/3}$ and therefore the small departures from the "perfect" correlation in V_s are amplified when they enter τ_{Ee}. This is a classical case of error propagation.

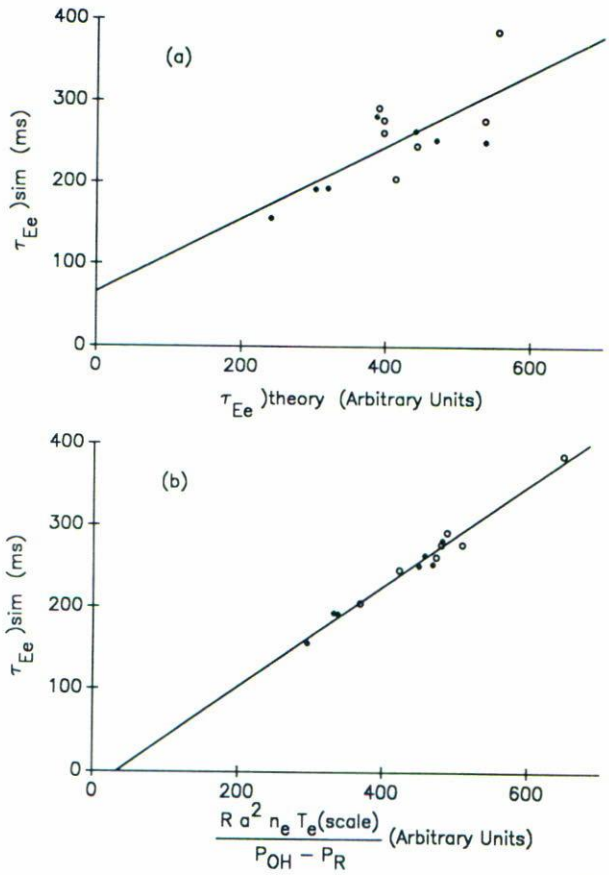

FIGURE 4. Simulation electron energy confinement time compared with (a) the predicted scaling from the theory for τ_{Ee} (obtained if only electron energy diffusion were responsible for all transport); and (b) an intermediate predicted scaling obtained from the temperature scaling given by the theory (T_e(scale) from Eq. (9)) and the relation $a^2 R n_e T_e(\text{scale})/(P_{OH} - P_R)$. Correlation coefficient for the first case is 0.73, whereas for the second it is as good as 0.99.

Owing to the fact that τ_{Ee} is a quantity that is computed from various fundamental parameters that are directly measurable, it is to be expected that the spreading about a certain scaling not be small due to the amplification of fitting errors, even if the scaling is correct. This is actually what we obtain in Figs. 3(b) and 4(a). Thus, both scalings (10) and (12) may be adequate for τ_{Ee} but we cannot favor one over the other on the basis of our results. It could even be that both scalings, the experimental and the theoretical, coincide to certain extent if the latter could be expressed in a simple form containing only "basic" plasma parameters. In any case, it is clear that one cannot distinguish between two different scalings that give plots with similar spreadings, based on this analysis. This statement, combined with the fact that there are many possible forms of χ_e^{an} that produce the same

τ_{Ee} scaling, leads us to the following conclusion. The scalings found experimentally for the energy confinement time can be helpful for empirical predictions of future trends in machine design, but they cannot provide much information about the scaling of χ_e^{an} [26].

The results about the relation between the scalings and the numerical results just described are independent of the presence of sawtooth oscillations within the model we used for them. This was tested by repeating the simulations but suppressing all sawtooth activity. The major effect of the sawtooth switch-off was to increase the central temperatures making the profiles more peaked, as one would expect, but the resulting correlations with the scalings of T_e, V_s and τ_{Ee} were almost unchanged. This result makes clear that sawteeth dominate the transport only in the central region of the plasma.

5. CONCLUSIONS

We have analyzed a series of Ohmic TFTR discharges covering a range of plasma conditions with high impurity content and therefore important fractions of radiation losses. They are reasonably well fit by a 1D transport simulation using an anomalous electron thermal diffusion based on the global constraint of profile consistency, together with the local stipulation of transport due to current-driven electrostatic modes. The diffusivity includes non-Ohmic energy terms, represented by impurity radiation in our case, and a normalization quantity associated with them. In determining this normalization it was found that the best results were obtained when the entire plasma column was involved in computing its value. This transport model represents the first step toward simulating auxiliary heated discharges, in which case it might be necessary to include the effects of finite β_p degradation.

The model employed is a good representation of the transport to a large scale and as such is suitable for transport simulations of the total plasma volume. In contrast, this models cannot give account of detailed transport processes at microscopic scales, such as those associated with the propagation of the energy pulse produced in a sawtooth crash. This simulations are relevant for understanding the relationship among different globally determined discharge quantities, such as τ_{Ee} and τ_E^{OH}, and local parameters (T_{e0}, V_s, q_a, etc.), in order to establish their relevance in characterizing the experiment.

In combination with a sawtooth crash model, the electrical resistivity was found to be neoclassical over all the plasma cross section. This agrees with the result of Ref. [14] also for TFTR, where they conclude that this evidences that the anomalous cross-field electron transport cannot come from an anomalous collision frequency. This would conflict with our assumption in Eq. (4), but since this is used just for locking the magnitude of χ_e^{an} it would not alter any conclusion regarding profile consistency. Electron temperature profiles were fit adequately by the assumed models. The central ion temperature was fairly fit by assuming a neoclassical ion

thermal transport, although there is some uncertainty in the available data. This finding can be contrasted with the results of recent TFTR simulations [11] based on the profile-consistent model Ref. [4] for χ_e^{an}, where they assume anomalous ion transport, and find that the ion temperatures are overestimated.

The presence of sawteeth was important in fitting the temperature profiles and in reproducing some of the characteristic features of profile consistency (r_d/a, $\langle T_e \rangle / T_{e0} \sim 1/q_a$), the latter in agreement with Refs. [5,6]. However, the resulting fit to the scalings are not sensitive to sawteeth.

The total energy confinement time from the simulations followed the experimentally determined scaling with $\bar{n}_e$ and q_a (the plasma dimensions were not varied). It also approximately follows the scaling implied by χ_e^{an}, but since this is not expressed in a simple way in terms of basic parameters it cannot be related to the empirical scaling. The agreement of τ_{Ee} with the predictions is not as good as in the cases of T_e and V_s, probably because the small mismatches are amplified in τ_{Ee}. This makes difficult to use the observed scalings of T_{ea} to predict scalings for χ_e^{an}.

It is interesting to mention that TFTR simulations with important impurity radiation losses were also performed by Redi *et al.* [8] using an extension of Tang's profile consistent model [4] to include these losses, and they found good agreement with the empirical scaling for τ_E^{OH} (Eq. (12)). It then appears that the property of profile consistency is of fundamental importance in fitting experimental results, even though the partial scalings of χ_e^{an} are different. The simplicity provided by profile consistency can be contrasted with the complication of models based on first-principle theories of anomalous transport, where different kind of processes have to be assumed for each region of the plasma, and then combined in a numerical code [27].

The important conclusion to be stressed is that the empirical scalings can be obtained from transport coefficients with different scalings, as long as their radial dependences are the result of profile consistency. We have shown this by including only impurity radiation as the non-Ohmic term in χ_e^{an}, to simulate Ohmic discharges with high radiation losses, and comparing with the simulations of Ref. [8] where the same situation is analyzed. This was done to simplify the analysis, avoiding finite beta effects associated with intense auxiliary heating. However, in view of the previous conclusion, we should expect to obtain good results when auxiliary heating is included in the present model, given that good fits have been found with the other profile consistent model [11].

ACKNOWLEDGMENTS

The author is grateful for the assistance of P.C. Efthimion and the TFTR group in providing and interpreting the experimental data. He also thanks B. Coppi and L. Sugiyama for many stimulating discussions and advice on the topics of this paper. The work was partially supported by UNAM-DGAPA project No. IN-100589.

REFERENCES

1. F.A. Haas and A. Thyagaraja, *Phys. Rep.* **143** (1986) 240;. P.C. Liewer, *Nucl. Fusion* **25** (1985) 543.
2. B. Coppi, *Comments Plasma Phys. Contl. Fusion* **5** (1980) 261; B. Coppi and E. Mazzucato, *Phys. Lett.* **A 71** (1979) 337.
3. D.A. Boyd and F.J. Stauffer, *Comments Plasma Phys. Contl. Fusion* **11** (1987) 63.
4. W.M. Tang, *Nucl. Fusion* **26** (1986) 1605.
5. E.D. Fredrickson, K.M. McGuire, R.J. Goldston, M.G. Bell, B. Grek, D.W. Johnson, A.W. Morris, F.J. Stauffer, G. Taylor and M.C. Zarnstorff, *Nucl. Fusion* **27** (1987) 1897.
6. V. Arunasalam, M.L. Bretz, P.C. Efthimion, R.J. Goldston, B. Grek, D.W. Johnson, M. Murakami, K.M. McGuire, D.A. Rasmussen, F.J. Stauffer and J.B. Wilgen, *Nucl. Fusion* **30** (1990) 2111.
7 F. Wagner, O. Gruber *et al., Phys. Rev. Lett.* **56** (1986) 2187; H. Renner *et al., Plasma Phys. Contl. Fusion* **26 1A** (1984) 183; A. Iiyoshi *et al., Phys. Rev. Lett* **48** (1982) 745.
8. M.H. Redi, W.M. Tang, P.C. Efthimion, D.R. Mikkelsen and G.L. Schmidt, *Nucl. Fusion* **27** (1987) 2001.
9. D.H. Humphreys and L. Sugiyama, *Shewood Theory Meeting*, Arlington VA, Paper IS26 (1983); B. Coppi and N. Sharky, *Comments Plasma Phys. Contl. Fusion* **7** (1982) 7.
10. O. Gruber, *Nucl. Fusion* **22** (1982) 1349.
11. M.H. Redi and G. Bateman, *Nucl. Fusion* **31** (1991) 547.
12. B. Coppi, *Fiz. Plazmy* **11** (1985) 83.
13. B.B. Kadomtsev, *Sov. J. Plasma Phys.* **1** (1975) 389.
14. M.C. Zarnstorff, K. McGuire, M.G. Bell, B. Grek, D. Johnson, D. McCune, H. Park, A. Ramsey and G. Taylor, *Phys. Fluids* **B 2** (1990) 1852.
15. C.S. Chang and F.L. Hinton, *Phys. Fluids* **25** (1982) 1493.
16. TFTR Database, communicated by P.C. Efthimion.
17. E. Westerhof, *Comments Plasma Phys. Contl. Fusion* **11** (1987) 79.
18. H. Yamada, K. McGuire *et al.*, Princeton Plasma Phys. Lab. Report PPPL-2213 (1985).
19. L. Sugiyama and R. Englade, RLE Report PTP-82/14, M.I.T. (1982).
20. G. Taylor, P.C. Efthimion *et al., Nucl. Fusion* **26** (1986) 339.
21. R.Z. Sagdeev, in *Advances in Plasma Physics*, Simon and Thompson (eds.), Interscience, Vol. 5 (1974) 153.
22. G. Becker *et al., Nucl. Fusion* **22** (1982) 1589.
23. B. Coppi and N. Sharky, *Nucl. Fusion* **21** (1981) 1363.
24. P.C. Efthimion *et al.* in *10th IAEA Conf. Plasma Phys. Contl. Nucl. Fusion Res.*, London **1** (1984) 29.
25. R.J. Hawriluk *et al.*, in *Heating in Toroidal Plasmas (Proc. 4th Symp. Intl. School Plasma Phys., Rome)* ENEA, Frascati (1984).
26. J.J. Martinell, Ph.D. Thesis, Massachusetts Institute of Technology (1986).
27. R.R. Domínguez and R.E. Waltz, *Nucl. Fusion* **27** (1987) 65.

RESUMEN. La simulación de varias descargas en TFTR, usando un código de transporte unidimensional, muestra una concordancia razonablemente buena con los experimentos cuando el transporte anómalo de energía electrónica se modela por una expresión de la difusividad térmica electrónica χ_e^{an} basada en el principio de consistencia de perfiles, generalizado para casos con contribuciones no óhmicas importantes en el balance de energía

para electrones, las cuales, en nuestro caso, son las pérdidas debidas a radiación de impurezas. Los parámetros involucrados en esta generalización de la difusividad térmica electrónica resultan tener los mismos valores que los determinados previamente para descargas óhmicas en otras máquinas tales como Alcator A y FT, siempre y cuando se suponga resistividad eléctrica neoclásica. El modelo de transporte da una buena descripción de descargas óhmicas con dominio electrónico en TFTR sobre un rango de densidades y corrientes del plasma. Para la mayoría de las descargas se encuentran ajustes relativamente buenos a los perfiles radiales de temperatura electrónica y voltajes en la superficie. Nuestros resultados muestran que el tiempo de confinamiento de energía total está de acuerdo con los escalamientos experimentales propuestos; también son consistentes con los escalamientos esperados del modelo empleado para el voltaje superficial y la temperatura electrónica. Se incluye la presencia de oscilaciones de diente de sierra y se encuentra que, para el modelo usado, tienen poco efecto en los ajustes a los escalamientos pero dominan el transporte en la región central del plasma, afectando ahí los perfiles.